Electronic Supplementary Material (ESI) for Analytical Methods.

Electronic supplementary information

Multi-scale magnetic nanoparticle based optomagnetic bioassay for sensitive DNA and bacteria detection

Bo Tian,[†] Teresa Zardán Gómez de la Torre,[‡] Marco Donolato,[§] Mikkel Fougt Hansen,[§] Peter Svedlindh,[†] and Mattias Strömberg*[,†]

[†] Department of Engineering Sciences, Division of Solid State Physics, Uppsala University, The Ångström Laboratory, Box 534, SE-751 21 Uppsala, Sweden

[‡] Department of Engineering Sciences, Division of Nanotechnology and Functional Materials, Uppsala University, The Ångström Laboratory, Box 534, SE-751 21 Uppsala, Sweden

[§] Department of Micro- and Nanotechnology, Technical University of Denmark, DTU Nanotech, Building 345 East, DK-2800 Kongens Lyngby, Denmark

* Corresponding author.

E-mail address: mattias.stromberg@angstrom.uu.se (M. Strömberg).
Phone: +46 18 471 3139.

S1. Optomagnetic system description and optomagnetic measurement principle.

As illustrated in **Fig. S1**, the set-up employed for optomagnetic effect measurement was based on an unfocused 405 nm laser source (Sony optical unit, Sony, JP) and a photodetector (PDA36A, Thorlabs Inc., U.S.A.). Powered by a software controlled current source, the laser source provided a linearly polarized light beam (diameter of 2 mm), and the polarization direction was oriented along the axis of the applied magnetic field. A disposable UV-transparent cuvette (REF 67.758.001, SARSTEDT, Nümbrecht, Germany) was positioned in the beam path, centred between a pair of electromagnets (1433428C, Murata Power Solutions Inc., U.S.A.). The optical path through the liquid in the cuvette was 10 mm. The distance between the electromagnets was 20 mm, and the distance between laser source and detector was 115 mm. The LabVIEW controlled electromagnets were powered by an AC source. The AC magnetic field was applied perpendicular to the laser beam, and the maximum AC magnetic field amplitude was limited to approximately 2.6 mT in the current set-up. The self-inductance of the electromagnets was corrected to ensure constant field amplitude and phase at all frequencies. The laser, electromagnets, cuvette, and detector were covered during measurements to avoid interference from external light sources. The detector signal was converted from analogue to digital by a data acquisition unit (DAQ unit, NI USB-6341, National Instruments, U.S.A.), followed by further processing in the computer by a FFT enabled lock-in function.

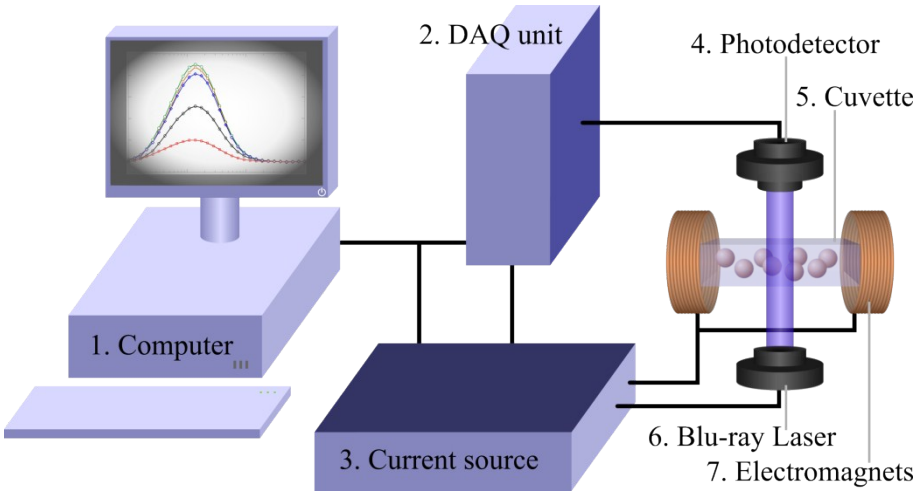

Fig. S1 Schematic illustration of the optomagnetic set-up. The liquid sample, contained in an optically transparent cuvette (5), is placed between two identical electromagnets (7). A 405 nm laser source (6) generates a laser beam aimed at the bottom of the cuvette. The transmitted light detected by a photo detector (4) is recorded vs. time using a DAQ unit (2). The laser and electromagnets are powered by a current source (3). A computer (1) controls the entire set-up and performs the software based lock-in detection.

The optomagnetic measurement principle is based on the rotational dynamics of magnetic nanoparticles (MNPs). The MNPs employed in this study have a remanent magnetic moment, which implies that the dominating relaxation mechanism upon a reversal of the magnetic field direction is a physical rotation of the particle, known as Brownian relaxation. The characteristic frequency for Brownian relaxation dynamics is given by

$$f_B = \frac{k_B T}{6\pi\eta V_h}, \tag{1}$$

where $k_B T$ is the thermal energy, η is the dynamic viscosity and V_h is the hydrodynamic volume of the relaxing entity (e.g., a single MNP). The dynamic magnetic behavior can be described in term of the magnetic susceptibility χ with real (in-phase) and imaginary (out-of-phase) parts χ' and χ'', respectively. In case of a sinusoidal magnetic field $h_0 \sin(\omega t)$, the time dependent linear magnetic response can be expressed as

$$\chi(t) = M(t)/h_0 = \chi_0 \sin(\omega t - \theta) = \chi' \sin(\omega t) + \chi'' \cos(\omega t), \tag{2}$$

where $\chi' = \chi_0 \cos(\theta)$ and $\chi'' = \chi_0 \sin(\theta)$. At low frequencies the MNPs are able to rotate and follow the magnetic field, and the response is in-phase with the applied field. Therefore χ' is maximal. The rotation of the MNPs starts to lag behind the applied field at higher frequencies, which leads to a decrease in the in-phase component χ' and a corresponding increase in the out-of-phase component χ''. The out-of-phase component χ'' attains its maximum value at the Brownian relaxation frequency f_B.

A simple approach to account for a distribution of MNP sizes was introduced by Cole and Cole[1] according to the following expression for the complex magnetic susceptibility

$$\chi(\omega) - \chi_\infty = \frac{\chi_0 - \chi_\infty}{1 + (i\omega\tau_B)^{1-\alpha}}, \tag{3}$$

where α is the Cole-Cole parameter (ranging from 0 to 1, a measure of the nanoparticle size distribution width), $\tau_B = (f_B)^{-1}$ is the Brownian relaxation time, $\omega = 2\pi f$ is the angular frequency of the applied field and χ_0 and χ_∞ are the zero and infinity frequency limits of χ.

The dynamics is determined by the rotational behavior of the individual MNPs, which follows the Brownian relaxation dynamics. The modulation of the transmitted light is found in the complex second harmonic voltage output from the photodetector

$$V_2 = V_2' + \mathrm{i}V_2'', \tag{4}$$

where V_2' and V_2'' are the in-phase and out-of-phase signals, respectively. The modulation is measured using a lock-in amplifier with the AC magnetic field excitation as reference. From the perspective of transmitted light, the MNP ensemble will scatter light equally for a positive and negative magnetic field of the same amplitude. We therefore assume that the photodetector signal can be described as

$$V(t) = V_0 + V_{AC}\left|\sin(\omega t - \theta)\right| = V_0 + c\chi_0\left|\sin(\omega t - \theta)\right|, \tag{5}$$

where V_0 represents the un-modulated part of the transmitted light (used here for normalization), $V_{AC} = c\chi_0$ is the amplitude of the frequency dependent signal and c is a constant. The photodetector signal can further be expressed using the Fourier series for $|\sin(\omega t - \theta)|$, yielding

$$V(t) = V_0 + c\chi_0\left[\frac{2}{\pi} - \frac{4}{\pi}\left(\frac{1}{3}\cos(2\omega t - 2\theta) + \frac{1}{15}\cos(4\omega t - 4\theta) + \ldots\right)\right]. \quad (6)$$

Specifically, the second harmonic signal is given by

$$\begin{aligned} V_2(t) &= -\frac{4c\chi_0}{3\pi}\cos(2\omega t - 2\theta) \\ &= -\frac{4c\chi_0}{3\pi}\left(\cos(2\omega t)\cos(2\theta) + \sin(2\omega t)\sin(2\theta)\right) \\ &= -\frac{4c\chi_0}{3\pi}\left(\cos(2\omega t)\left(\cos^2(\theta) - \sin^2(\theta)\right) + 2\sin(2\omega t)\sin(\theta)\cos(\theta)\right) \\ &= -\frac{4c\chi_0}{3\pi}\left(\cos(2\omega t)\left((\tilde{\chi}')^2 - (\tilde{\chi}'')^2\right) + 2\sin(2\omega t)\tilde{\chi}''\tilde{\chi}'\right) \end{aligned} \quad (7)$$

,

where $\tilde{\chi}' = \chi'/\chi_0$ and $\tilde{\chi}'' = \chi''/\chi_0$. The lock-in detected in-phase and out-of-phase components of the second harmonic signal therefore become (rms values)

$$\begin{aligned} V_2' &= -2V_2(0)\tilde{\chi}''\tilde{\chi}' \\ V_2'' &= -V_2(0)\left((\tilde{\chi}')^2 - (\tilde{\chi}'')^2\right) \end{aligned} \quad (8)$$

where $V_2(0) = 4c\chi_0/3\sqrt{2}\pi$ is the zero frequency limit of V_2 (and V_2'').

The sign of V_{AC} depends on the optical scattering properties and the measurement geometry. For a geometry where the transmission is measured perpendicular to the axis of the applied magnetic field, as used in the present study, it is generally found that V_{AC} is negative for MNPs with sizes smaller than about 130 nm for blue laser light (λ = 405 nm). For even larger scattering entities, V_{AC} first becomes positive (e.g., for 250 nm MNPs) and then negative (e.g.,

for 500 nm MNPs). This originates from the oscillation of the scattering cross-section with particle size as can be accounted for by Mie scattering theory.

In **Fig. S2a**, the normalized in-phase and out-of-phase components of the magnetic susceptibility, extracted from the Cole-Cole model, are plotted versus frequency. In **Fig. S2b**, normalized $\tilde{\chi}'\tilde{\chi}''$ and $(\tilde{\chi}')^2-(\tilde{\chi}'')^2$, have been plotted versus frequency to illustrate the shape of the two photodetector signals. The input susceptibilities, $\tilde{\chi}'$ and $\tilde{\chi}''$, are those displayed in **Fig. S2a**.

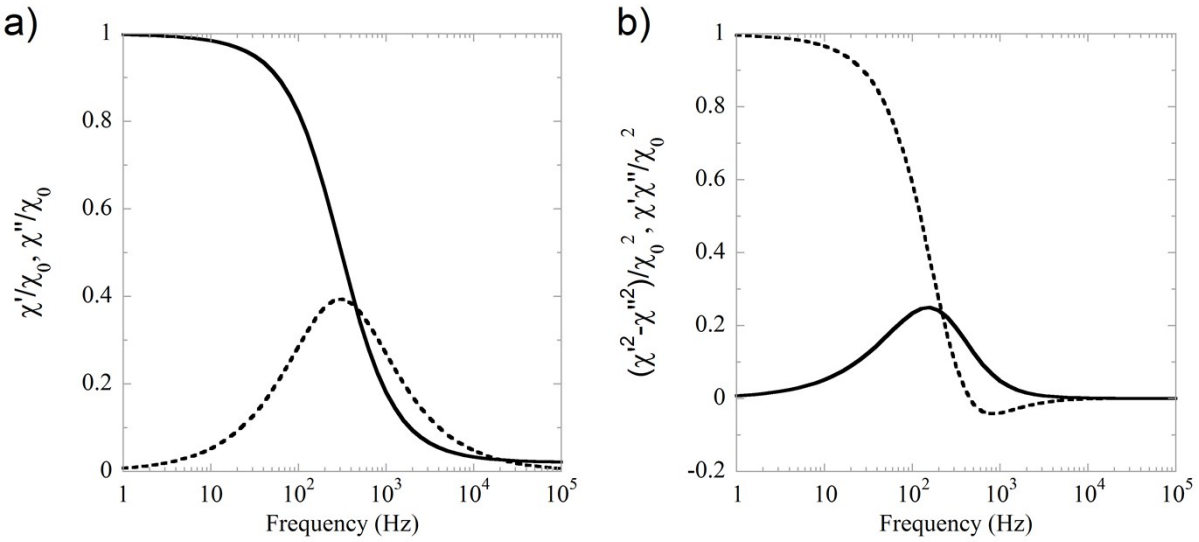

Fig. S2 (a) Normalized susceptibility data (in-phase and out-of-phase represented by solid and dashed lines, respectively) extracted from the Cole-Cole model versus frequency (τ_B =300 s and α =0.15 were used as input). (b) Normalized $\tilde{\chi}'\tilde{\chi}''$ (solid line) and $(\tilde{\chi}')^2-(\tilde{\chi}'')^2$ (dashed line) versus frequency. The $\tilde{\chi}'\tilde{\chi}''$ curve represents the in-phase signal from the photodetector, whereas the $(\tilde{\chi}')^2-(\tilde{\chi}'')^2$ curve represents the out-of-phase signal from the photodetector.

Table S1 Sequences of targets, padlock probes and detection oligonucleotides for *V. cholerae* (VC) and *E. coli* (EC).

Name	Sequence
Vibrio cholerae target (VC)	**5'-**CCCTGGGCTCAACCTAGGAATCGCATTTG**-3'**
Escherichia coli target (EC)	**5'-**ACGTCGCAAGACCAAAGAGGGGGACCT**-3'**
Padlock probe for VC	**5'-**TAGGTTGAGCCCAGGGACTTCTAGAGTGTACCGACCTCAGTAGCCG TGACTATCGACTTGTTGATGTCATGTGTCGCACCAAATGCGATTCC**-3'**
Padlock probe for EC	**5'-**CTTTGGTCTTGCGACGTCAGTGGATAGTGTCTTACACGATTTAG AGTGTACCGACCTCAGTAGCCGTGACTATCGACTAGGTCCCCCT**-3'**
Detection probe for VC	Biotin**-5'-**TTTTTTTTTTTTTTTTTTTTGTTGATGTCATGTGTCGCAC**-3'**
Detection probe for EC	Biotin**-5'-**TTTTTTTTTTTTTTTTTTTTGTGGATAGTGTCTTACACGA**-3'**

S2. Protocols for conjugation of detection oligonucleotide probes to MNPs. Streptavidin modified 100 nm MNPs were washed twice and resuspended in 1×Wtw buffer (10 mM Tris-HCl pH 8.0, 5 mM EDTA, 0.1% Tween20, 0.1 M NaCl) before conjugation. Biotinylated *V. cholerae* detection probes (1 μM) and streptavidin modified 100 nm MNPs (10 mg/mL) were mixed in a volumetric ratio of 5:8 followed by incubation at 37°C for 30 min. Thereafter the MNPs were washed twice using a magnetic separation stand, and resuspended at a concentration of 10 mg/mL in PBS.

The *E. coli* detection probe conjugated 250 nm MNPs were prepared following the same protocol as for the 100 nm MNPs except for that the *E. coli* detection probes (10 μM) and streptavidin modified 100 nm MNPs (10 mg/mL) were mixed in a volumetric ratio of 1:2. Detection probe conjugated MNPs were stored at 4°C for further use.

S3. Protocols for conjugation of antibodies to MNPs. For the "bacteria model" immunoassay, biotinylated goat anti avidin antibodies were conjugated to avidin modified

5 µm MPs by mixing biotinylated goat anti avidin antibody (1 mg/mL) and 5 µm MPs (25 mg/mL, 3.5×10^8 particles/mL) in a volumetric ratio of 2:1 followed by incubation at 37°C for 1 h. After incubation and washing twice using a magnetic separation stand, the Ab-MPs were resuspended at a concentration of 25 mg/mL (3.5×10^8 particles/mL) in PBS.

For the *Salmonella* immunoassay, antibody-conjugated 100 nm MNPs were prepared by mixing biotinylated rabbit anti *Salmonella* group antibody (4 mg/mL) and 100 nm streptavidin modified MNPs (10 mg/mL) in a volumetric ratio of 3:4 followed by incubation at 37°C for 2 h. After washing twice, the Ab-MNPs were resuspended at a concentration of 10 mg/mL in PBS.

To block the protein A groups on the surface of 250 nm MNPs, rabbit anti *E. coli* antibody (4 mg/mL, irrelevant antibody, AbD Serotec) and 250 nm protein A modified MNPs (10 mg/mL) were mixed in a volumetric ratio of 3:4 followed by incubation at 37°C for 2 h. After washing twice, blocked MNPs were resuspended at a concentration of 10 mg/mL in PBS. Ab-MPs and Ab-MNPs were stored at 4°C for further use.

S4. Protocols for padlock probe target recognition, ligation and rolling circle amplification. Ligation mix (20 nM) was prepared by mixing 10×phi29 DNA polymerase buffer, ATP (20 mM), phosphorylated padlock probe (1 µM), target DNA sequence (1 µM), T4 DNA ligase (1 U/µL) and MilliQ water in a volumetric ratio of 10:5:2:6:2:75, followed by incubation at 37ºC for 15 min.

RCA mix was prepared by mixing ligation mix (20 nM), 10×phi29 DNA polymerase buffer, dNTP (2.5 mM), BSA (2 µg/µL), phi29 DNA polymerase (10 U/µL) and Milli-Q water in a volumetric ratio of 10:3:2:3:1:11, followed by incubation at 37ºC for 1 h and thereafter

inactivation at 65ºC for 5 min. RCA mix and hybridization buffer (0.1 M Tris-HCl pH 8.0, 0.1 M EDTA, 0.5% Tween-20 and 2.5 M NaCl) were mixed in a volumetric ratio of 3:17 to obtain 1 nM DNA coil solutions.

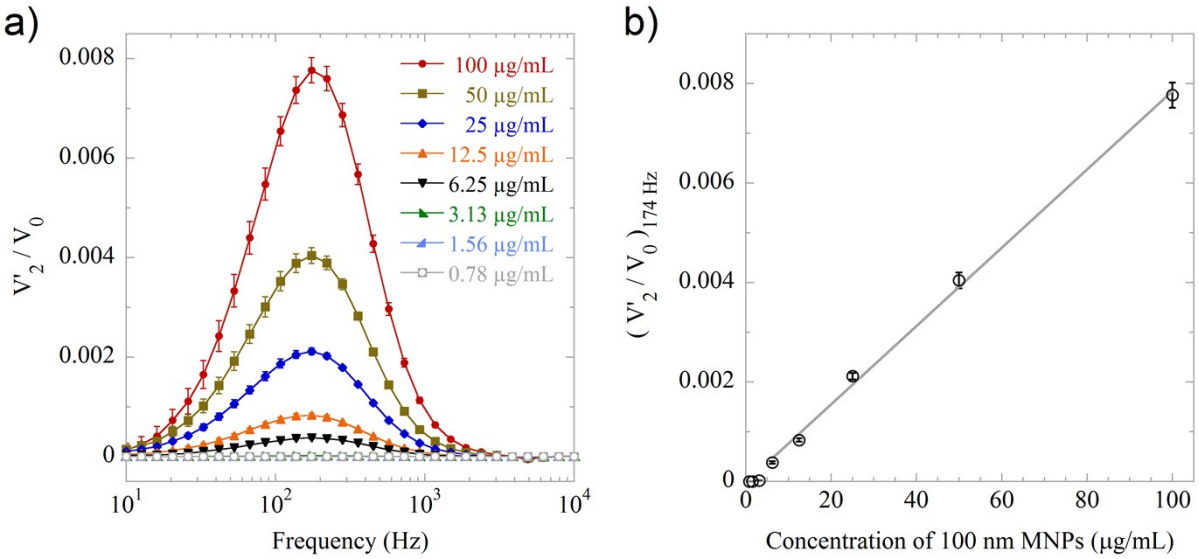

Fig. S3 Results of experiments carried out using unoptimized detection strategy (no blocking, no consideration of photodetector saturation, no addition of 250 nm MNPs). (a) V_2'/V_0 spectra of different concentrations of streptavidin coated 100 nm MNPs. (b) Corresponding value of $(V_2'/V_0)_{174\,\mathrm{Hz}}$ vs. $c_{100\,\mathrm{nm}}$. The grey line indicates the linear range. Error bars indicate one standard deviation based on three independent measurements.

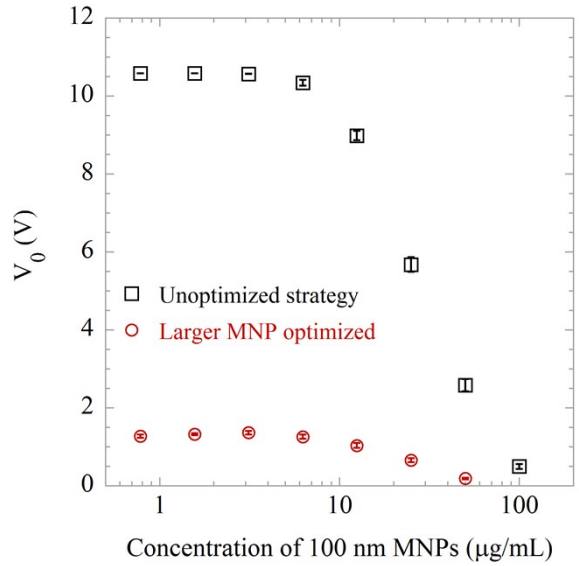

Fig. S4 Total intensity of transmitted laser light, V_0, vs. $c_{100\,\mathrm{nm}}$ without or with 50 μg/mL 250 nm MNPs, respectively. The data obtained for the unoptimized detection strategy are shown in Fig. S3. The saturation effect exists in the classical strategy when V_0 is approaching 10.6 V. Error bars indicate one standard deviation based on three independent measurements.

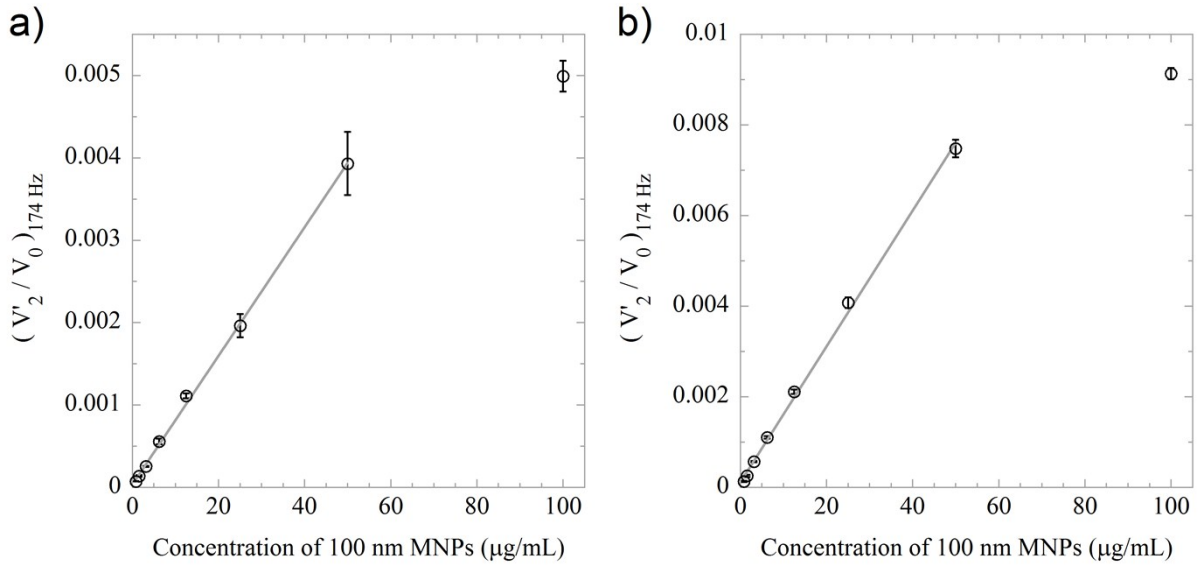

Fig. S5 (a) Corresponding value of $(V_2'/V_0)_{174\,\mathrm{Hz}}$ vs. $c_{100\,\mathrm{nm}}$, a filter was employed to reduce the intensity of laser beam. (b) Corresponding value of $(V_2'/V_0)_{174\,\mathrm{Hz}}$ vs. $c_{100\,\mathrm{nm}}$, the measurement was performed in a PBS buffer containing 0.1% BSA. The grey lines indicate the linear range. Error bars indicate one standard deviation based on three independent measurements.

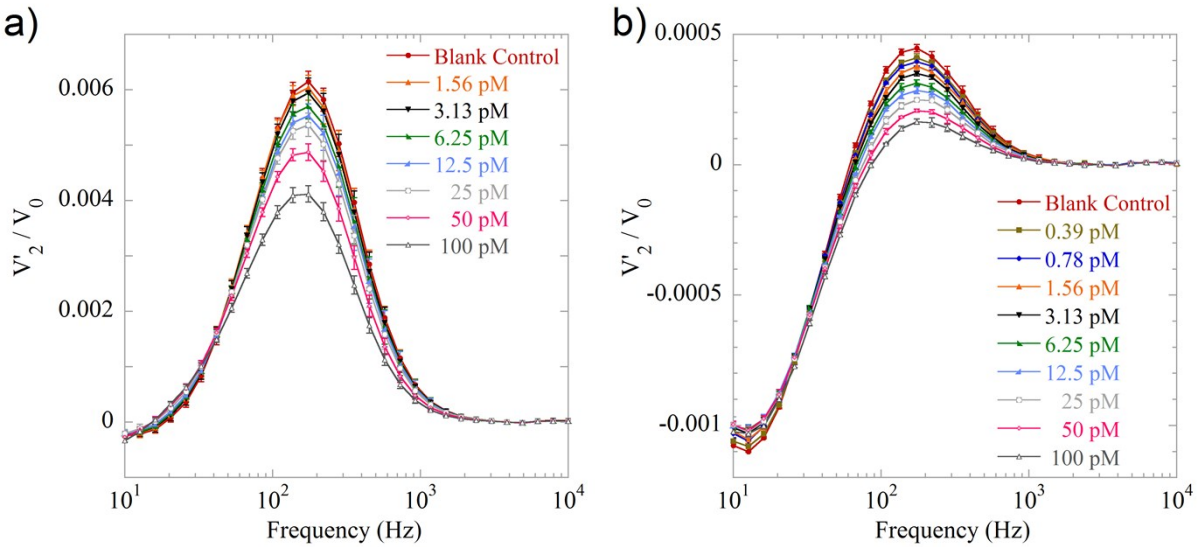

Fig. S6 (a) V_2'/V_0 spectra for the indicated concentrations of DNA coils by using detection strategy I. (b) V_2'/V_0 spectra for the indicated concentrations of DNA coils by using detection strategy II. Error bars indicate one standard deviation based on three independent measurements.

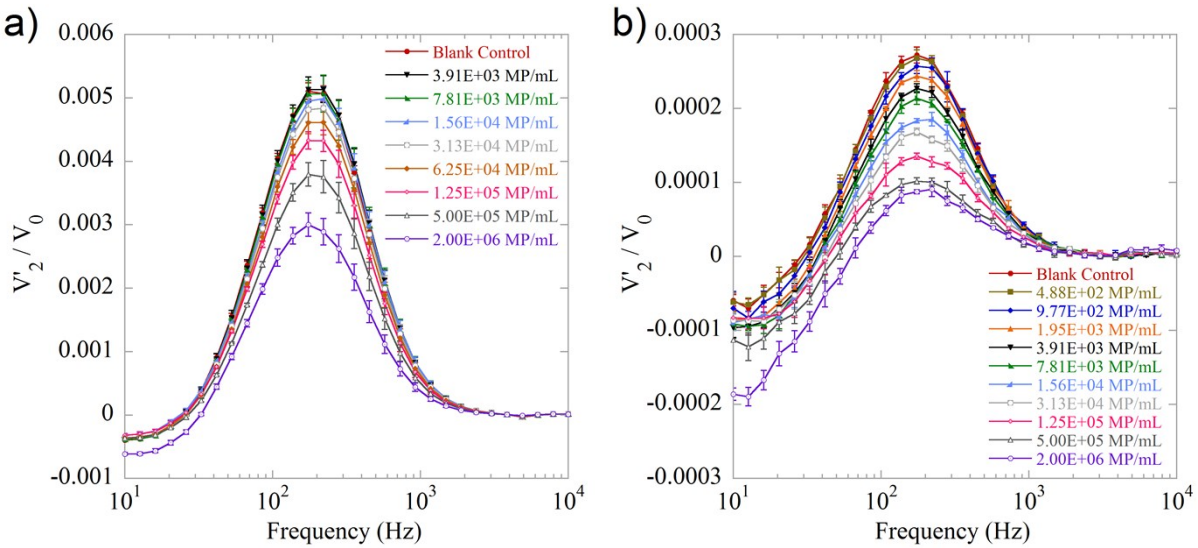

Fig. S7 (a) V_2'/V_0 spectra for the indicated concentrations of MPs (acting as "bacteria model") by using detection strategy I. (b) V_2'/V_0 spectra for the indicated concentrations of MP by using detection strategy II. Error bars indicate one standard deviation based on three independent measurements.

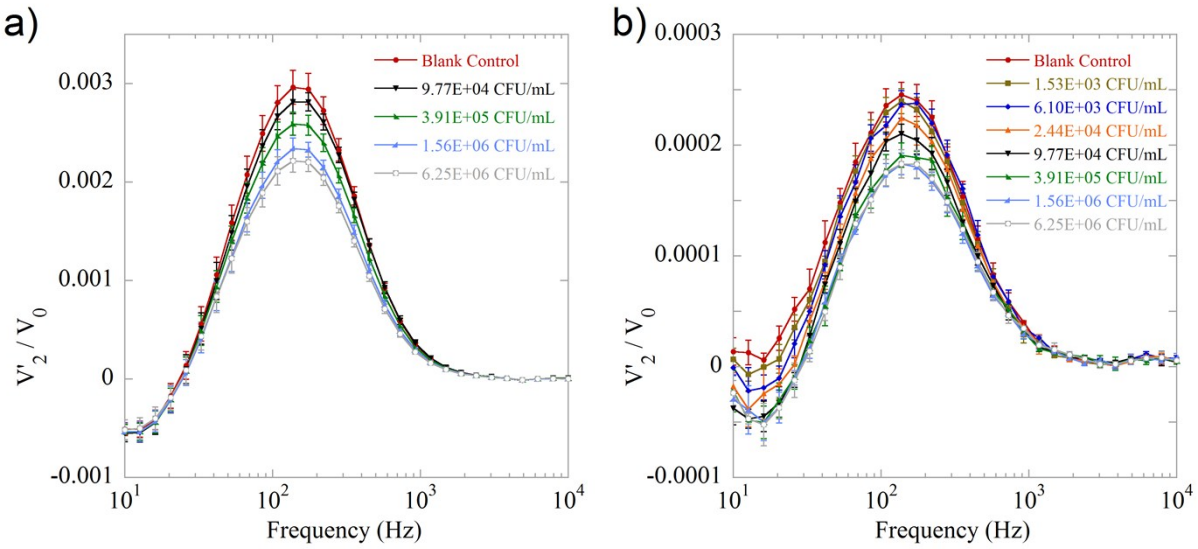

Fig. S8 (a) V_2'/V_0 spectra for the indicated concentrations of *Salmonella* by using detection strategy I. (b) V_2'/V_0 spectra for the indicated concentrations of *Salmonella* by using detection strategy II. Error bars indicate one standard deviation based on three independent measurements.

References

1 K. S. Cole and R. H. Cole, *J. Chem. Phys.*, 1941, **9**, 341-351.